Wideband Millimeter-wave OFDM Uplink with Hybrid Receiving

Yang Li and Anzhong Hu
School of Communication Engineering
Hangzhou Dianzi University
Hangzhou, China
Email: 2769761071@qq.com, huaz@hdu.edu.cn.

***Abstract*—In this paper, we study millimeter-wave orthogonal frequency division multiplexing uplink transmission with a wide bandwidth and hybrid receiving. By considering the spatial- and frequency-wideband effects in the channel model, the spectral efficiency of the system is analyzed. The analysis and the simulation results show the beam squint effect caused by the wideband effects. Moreover, the impacts of the bandwidth and the number of subcarriers on the beam squint effect are revealed.**

***Keywords*—Millimeter-wave (mm-wave), wideband, beam squint, orthogonal frequency division multiplexing (OFDM), hybrid.**

I. Introduction

A large antenna array and a wide bandwidth can be employed in millimeter-wave (mm-wave) communication to increase the data transmission rate. In such systems, the delay for each path at the base station (BS) antennas not only causes the phase differences between antennas, but also causes a non-negligible delay in the channel impulse response for the wide bandwidths. This is known as the spatial-wideband effect. As a result, the beam formed by the BS points to different direction for different frequencies. This is known as the beam squint effect and will be investigated in this paper.

In [1]- [3], channel estimation approaches are proposed to address the beam squint effect in wideband mm-wave systems. In [4], the transmission issues related to the beam squint effect is discussed. However, the spectral efficiency of the wideband mm-wave systems with hybrid receiving has not been analyzed in these papers. In [5], the signal-to-interference-plus-noise ratio (SINR) in wideband mm-wave systems is analyzed and shows the impacts of the array dimension and the bandwidth on the beam squint effect, but the dual-wideband effects, i.e., the spatial- and frequency-wideband effects, have not been considered in the analysis. On the other hand, the spectral efficiency of mm-wave systems is analyzed in [6]- [9]. However, these analyses have not addressed the beam squint effect in wideband mm-wave systems.

In this paper, the spectral efficiency of wideband mm-wave orthogonal frequency division multiplexing (OFDM) uplink transmission with hybrid receiving is analyzed. The base station (BS) is equipped with a large array and employs a hybrid receiving structure. The dual-wideband effects are considered in the channel model. By analyzing the norm of the beamspace channel, the spectral efficiency of the system is derived, which shows the deterioration caused by the beam squint effect. Moreover, the impacts of the bandwidth and the number of subcarriers on the beam squint effect are revealed by analyzing the spectral efficiency, which provide guidance for designing the system.

This research was supported by Project LY20F010007 supported by Zhejiang Provincial Natural Science Foundation of China.

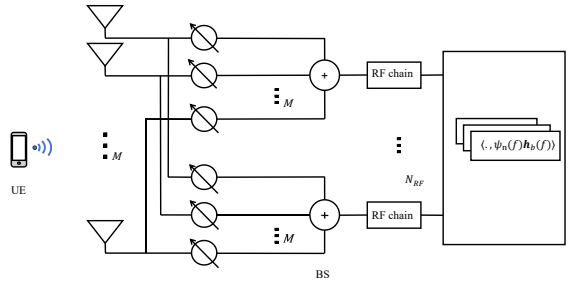

Fig. 1. A mm-wave uplink system where one single-antenna UE transmits OFDM signals to the BS with M antennas. The BS antennas are connected to a phase shift network and N_{RF} RF chains. In the digital processing unit, the signals are processed with matched filters.

Notations: Lower-case (upper-case) boldface symbols denote vectors (matrices); $\mathbf{A}^H$ is the conjugate transpose of $\mathbf{A}$; $[\mathbf{a}]_m$ is the m-th element in $\mathbf{a}$; $[\mathbf{A}]_m$ is the m-th column in $\mathbf{A}$; $\|\mathbf{x}\|$ denotes the Euclidean 2-norm of a complex vector $\mathbf{x}$; $\mathbb{E}\{\cdot\}$ is the expectation; $\delta(\cdot)$ is the Dirichlet delta function; $\mathbf{I}_M$ is an identity matrix with dimension M; $a(t)*b(t)$ is the convolution of $a(t)$ and $b(t)$; $\langle \mathbf{a}(f), \mathbf{b}(f)\rangle = \int_{f_1}^{f_2} \mathbf{b}^H(f)\mathbf{a}(f)\mathrm{d}f$ is the inner product, where $[f_1, f_2]$ is the range of the frequency.

II. System Model

The considered system is depicted in Fig. 1. In this system, a user equipment (UE) with an antenna is transmitting signals to the BS. The BS is equipped with a uniform linear array of M antennas. The BS antennas are connected to a phase shift network which conducts analog receiving. The phase shift

network is connected to N_{RF} radio frequency (RF) chains. The received signal at the BS at the t-th slot can be expressed as

$$\mathbf{y}(t) = x(t) * \mathbf{h}(t) + \mathbf{n}(t) \in \mathbb{C}^{M\times 1}, \quad (1)$$

where $x(t)$ is the transmitted signal, $\mathbf{h}(t) \in \mathbb{C}^{M\times 1}$ is the channel between the UE and the BS, $\mathbf{n}(t) \in \mathbb{C}^{M\times 1}$ is the received noise. As the system works with wide bandwidths and mm-wave bands, the channel is of multipaths and is frequency selective. By considering the dual wideband effects, the m-th element of the channel vector can be expressed as

$$[\mathbf{h}(t)]_m = \sum_{l=1}^{L} \alpha_l e^{-j2\pi(m-1)\theta_l} \times W\mathrm{sinc}\left(W\left(t-(m-1)\theta_l/f_{\mathrm{c}}-\tau_l\right)\right), \quad (2)$$

where α_l is the complex path gain of the l-th path which is complex Gaussian distributed with mean zero and variance σ_α^2, τ_l is the time delay of the l-th path, W is the bandwidth, L is number of paths, f_{c} is the carrier frequency. As the array is linear, we have $\theta_l = d/\lambda \sin(\phi_l)$, where ϕ_l is the direction-of-arrival (DOA) of the l-th path, λ is the wavelength, d is the distance between adjacent BS antennas.

In order to simplify the BS structure and save power in mm-wave systems with large arrays, the hybrid structure is employed at the BS. The received signal is first processed with analog beamforming, which is further converted to the digital domain with RF chains. There are N_{RF} RF chains, which means N_{RF} analog beamforming vectors are employed. The analog beamforming vector $\mathbf{a}(\bar{\theta}_n) \in \mathbb{C}^{M\times 1}$ is defined as

$$[\mathbf{a}(\bar{\theta}_n)]_m = \frac{1}{\sqrt{M}} e^{-j2\pi(m-1)\bar{\theta}_n},$$

where

$$\bar{\theta}_n = \frac{1}{M}\left(n-1-\frac{M-1}{2}\right).$$

The vectors with $n = 1, 2, \cdots, M$ form into $\mathbf{U} \in \mathbb{C}^{M\times M}$ in which

$$[\mathbf{U}]_n = \mathbf{a}\left(\bar{\theta}_n\right). \quad (3)$$

In this system, N_{RF} beams are selected, i.e., N_{RF} columns of $\mathbf{U}$ are selected and formed into $\mathbf{U}_{\mathrm{b}} \in \mathbb{C}^{M\times N_{\mathrm{RF}}}$. It can be seen that $\mathbf{U}^H\mathbf{U} = \mathbf{I}_M$, $\mathbf{U}_{\mathrm{b}}^H\mathbf{U}_{\mathrm{b}} = \mathbf{I}_{N_{\mathrm{RF}}}$.

With $\mathbf{U}_{\mathrm{b}}$, the received signal can be converted into the beamspace as

$$\begin{aligned} \mathbf{y}_{\mathrm{b}}(t) &= \mathbf{U}_{\mathrm{b}}^H\mathbf{y}(t) & (4)\\ &= x(t) * \mathbf{h}_{\mathrm{b}}(t) + \mathbf{n}_{\mathrm{b}}(t) \in \mathbb{C}^{N_{\mathrm{RF}}\times 1}, & (5)\end{aligned}$$

where (5) is obtained by substituting (1) into (4), and

$$\begin{aligned} \mathbf{h}_{\mathrm{b}}(t) &= \mathbf{U}_{\mathrm{b}}^H\mathbf{h}(t) \in \mathbb{C}^{N_{\mathrm{RF}}\times 1}, & (6)\\ \mathbf{n}_{\mathrm{b}}(t) &= \mathbf{U}_{\mathrm{b}}^H\mathbf{n}(t) \in \mathbb{C}^{N_{\mathrm{RF}}\times 1}. & (7)\end{aligned}$$

Substituting (2) and (3) into (6) yields

$$[\mathbf{h}_{\mathrm{b}}(t)]_s = \frac{1}{\sqrt{M}} \sum_{l=1}^{L}\sum_{m=1}^{M} \alpha_l e^{-j2\pi(m-1)(\theta_l-\bar{\theta}_{g(s)})} \times W\mathrm{sinc}\left[W(t-(m-1)\theta_l/f_{\mathrm{c}}-\tau_l)\right], \quad (8)$$

where $s = 1, 2, \cdots, N_{\mathrm{RF}}$, $g(s)$ is the column index of $[\mathbf{U}_{\mathrm{b}}]_s$ in $\mathbf{U}$. Denote the Fourier transform of $\mathbf{n}(t)$ as $\tilde{\mathbf{n}}(f) \in \mathbb{C}^{M\times 1}$. We assume that

$$\mathbb{E}\{\tilde{\mathbf{n}}(f)\tilde{\mathbf{n}}^H(f')\} = \frac{N_0}{2}\delta(f-f')\mathbf{I}_M. \quad (9)$$

Correspondingly, the frequency domain expression of the received signal $\mathbf{y}_{\mathrm{b}}(t)$ is written as

$$\tilde{\mathbf{y}}_{\mathrm{b}}(f) = \tilde{x}(f)\tilde{\mathbf{h}}_{\mathrm{b}}(f) + \tilde{\mathbf{n}}_{\mathrm{b}}(f), \quad (10)$$

where $\tilde{x}(f)$ is the Fourier transform of $x(t)$, and $\tilde{\mathbf{h}}_{\mathrm{b}}(f) \in \mathbb{C}^{N_{\mathrm{RF}}\times 1}$ is the Fourier transform of $\mathbf{h}_{\mathrm{b}}(t)$, and $\tilde{\mathbf{n}}_{\mathrm{b}}(f) \in \mathbb{C}^{N_{\mathrm{RF}}\times 1}$ is the Fourier transform of $\mathbf{n}_{\mathrm{b}}(t)$. According to (8), we have

$$\begin{aligned} [\tilde{\mathbf{h}}_{\mathrm{b}}(f)]_s &= \frac{1}{\sqrt{M}} \sum_{l=1}^{L}\sum_{m=1}^{M} \alpha_l e^{-j2\pi(m-1)(\theta_l-\bar{\theta}_{g(s)})} \\ &\times \int_{-\infty}^{\infty} W\mathrm{sinc}\left[W(t-(m-1)\theta_l/f_{\mathrm{c}}-\tau_l)\right] e^{-j2\pi ft}\mathrm{d}t \\ &= \frac{1}{\sqrt{M}} \sum_{l=1}^{L}\sum_{m=1}^{M} \alpha_l e^{-j2\pi(m-1)(\check{\theta}_l(f)-\bar{\theta}_{g(s)})} e^{-j2\pi\tau_l f} \\ &= \frac{1}{\sqrt{M}} \sum_{l=1}^{L} \alpha_l e^{-j2\pi f\tau_l} G(\check{\theta}_l(f)-\bar{\theta}_{g(s)}) \\ &\times e^{j\pi(M-1)(\check{\theta}_l(f)-\bar{\theta}_{g(s)})}, \end{aligned} \quad (11)$$

where $\check{\theta}_l(f) = \theta_l(f/f_{\mathrm{c}}+1)$,

$$G(\check{\theta}_l(f)-\bar{\theta}_{g(s)}) = \frac{\sin\left((\check{\theta}_l(f)-\bar{\theta}_{g(s)})M\right)}{\sin\left(\check{\theta}_l(f)-\bar{\theta}_{g(s)}\right)}. \quad (12)$$

According to (7), we have

$$\begin{aligned} \mathbb{E}\{\tilde{\mathbf{n}}_{\mathrm{b}}(f)\tilde{\mathbf{n}}_{\mathrm{b}}^H(f')\} &= \mathbf{U}_{\mathrm{b}}^H\mathbb{E}\{\tilde{\mathbf{n}}(f)\tilde{\mathbf{n}}^H(f')\}\mathbf{U}_{\mathrm{b}} \\ &= \frac{N_0}{2}\delta(f-f')\mathbf{I}_{N_{\mathrm{RF}}}, \end{aligned} \quad (13)$$

where (9) and the orthogonality property under (3) are employed in deriving (13).

A. OFDM Symbols

The transmitted signals are OFDM modulated as

$$x(t) = \sum_{n=0}^{N-1} x_n\psi_n(t),$$

where $x_n, n = 0, 1, \cdots, N-1$ are independent random symbols with $\mathbb{E}\{|x_n|^2\} = \mathrm{E_x}$, $\psi_n(t), n = 0, 1, \cdots, N-1$ are the orthogonal waveforms given as

$$\psi_n(t) = \frac{1}{\sqrt{T}} e^{j2\pi f_n t}, 0 \le t \le T,$$

where N is the number of subcarriers, T is the duration of the waveform. Correspondingly, the subcarrier in the the frequency domain is expressed as

$$\tilde{\psi}_n(W, f) = \frac{e^{j2\pi(f_n-f)T}-1}{j2\pi(f_n-f)\sqrt{T}}, \quad (14)$$

where $-\frac{W}{2} \leq f \leq \frac{W}{2}$, $T = N/W$, W is the bandwidth of $x(t)$, f_n is the center frequency of each subcarrier. Thus, the inter-subcarrier difference is $B = W/(N+1)$, and $f_n = -W/2 + nB$. Then, we have

$$\tilde{x}(f) = \sum_{n=0}^{N-1} x_n \tilde{\psi}_n(W, f). \tag{15}$$

B. Beam Selection

Assume the channel $\mathbf{h}(t)$ is known, according to (11), we have the channel in the beamspace and the frequency domain as $\tilde{\mathbf{h}}_{\mathrm{ba}}(f) \in \mathbb{C}^{B\times 1}$, where

$$[\tilde{\mathbf{h}}_{\mathrm{ba}}(f)]_n = \frac{1}{\sqrt{M}} \sum_{l=1}^{L} \alpha_l e^{-j2\pi f \tau_l} G(\check{\theta}_l(f) - \bar{\theta}_n) \times e^{j\pi(M-1)(\check{\theta}_l(f)-\bar{\theta}_n)},$$

$n = 1, 2, \cdots, N$. Then, the beams corresponding to the largest N_{RF} values of $|[\tilde{\mathbf{h}}_{\mathrm{ba}}(0)]_n|$ should be selected, and the indices of these beams are $g(s), s = 1, 2, \cdots, N_{\mathrm{RF}}$.

C. Matched Filter

Substituting (15) into (10) yields

$$\tilde{\mathbf{y}}_{\mathrm{b}}(f) = \sum_{n=0}^{N-1} x_n \tilde{\psi}_n(W, f) \tilde{\mathbf{h}}_{\mathrm{b}}(f) + \tilde{\mathbf{n}}_{\mathrm{b}}(f).$$

After converting the digital domain with the RF chains, for the n-th subcarrier, the matched filter (MF) receiver is employed, which results into

$$\begin{aligned} v_n &= \left\langle \tilde{\mathbf{y}}_{\mathrm{b}}(f), \tilde{\psi}_n(W, f) \tilde{\mathbf{h}}_{\mathrm{b}}(f) \right\rangle \\ &= x_n D_{n,n} + \sum_{n' \neq n} x_{n'} D_{n,n'} + z_n, \end{aligned} \tag{16}$$

where the signal and interference are expressed as

$$D_{n,n'} = \int_{-W/2}^{W/2} \tilde{\psi}_n^*(W, f) \tilde{\psi}_{n'}(W, f) ||\tilde{\mathbf{h}}_{\mathrm{b}}(f)||^2 \mathrm{d}f, \tag{17}$$

and the noise is

$$z_n = \int_{-W/2}^{W/2} \tilde{\psi}_n^*(W, f) ||\tilde{\mathbf{h}}_{\mathrm{b}}(f)||^2 \mathrm{d}f. \tag{18}$$

In this section, we have described the received signal, the channel, the OFDM symbols, the beam selection, and the matched filter. The system model in this paper is similar to that in [5], but is different in the consideration of the dual wideband effects, the employment of the OFDM, and the beam selection strategy. In the next section, we will analyze the spectral efficiency of the received signal with MF processing and show the effect of beam squint on the spectral efficiency.

III. Analysis of The Spectral Efficiency

In this section, we will first derive the spectral efficiency of the system, and then analyze the spectral efficiency to show the beam squint effect and the impacts of the system parameters.

According to (13) and (18), we have

$$\begin{aligned} \mathbb{E}\{|z_n|^2\} &= \frac{N_0}{2} \int_{-W/2}^{W/2} |\tilde{\psi}_n(W, f)|^2 ||\tilde{\mathbf{h}}_{\mathrm{b}}(f)||^2 \mathrm{d}f \\ &= \frac{N_0}{2} D_{n,n}, \end{aligned} \tag{19}$$

where (19) is derived with (17). Then, according to (16), the SINR of the n-th subcarrier is expressed as

$$\gamma_n = \frac{\mathrm{E_x} D_{n,n}^2}{\mathrm{E_x} \sum_{n' \neq n} D_{n,n'}^2 + \frac{N_0}{2} D_{n,n}}. \tag{20}$$

Correspondingly, the spectral efficiency of the system can be written as

$$R = \frac{1}{N} \sum_{n=1}^{N} \mathbb{E}\{\log_2(1 + \gamma_n)\}. \tag{21}$$

According to (11), we have

$$\begin{aligned} ||\tilde{\mathbf{h}}_{\mathrm{b}}(f)||^2 &= \frac{1}{M} \sum_{s=1}^{N_{\mathrm{RF}}} \Bigg| \sum_{l=1}^{L} \alpha_l e^{-j2\pi f \tau_l} \\ &\quad \times G(\check{\theta}_l(f) - \bar{\theta}_{g(s)})\, e^{j\pi(M-1)(\check{\theta}_l(f)-\bar{\theta}_{g(s)})} \Bigg|^2. \end{aligned}$$

Since the beams selected usually point to DOAs, we have $\check{\theta}_{p(s)}(0) \approx \bar{\theta}_{g(s)}$, where the s-th selected beam points to the $p(s)$-th path. As the number of BS antennas M is large and the beams are selected according to $|[\tilde{\mathbf{h}}_{\mathrm{ba}}(0)]_n|$, we have $G(\check{\theta}_l(f) - \bar{\theta}_{g(s)})/M \approx 0$ for $l \neq p(s)$. Thus, we have

$$||\tilde{\mathbf{h}}_{\mathrm{b}}(f)||^2 \approx \frac{1}{M} \sum_{s=1}^{N_{\mathrm{RF}}} \left| \alpha_{p(s)} G(\check{\theta}_{p(s)}(f) - \bar{\theta}_{g(s)}) \right|^2. \tag{22}$$

When the bandwidth W is narrow enough such that $\check{\theta}_{p(s)}(f)$ is almost invariant with the change of f in the domain $[-W/2, W/2]$, we can approximate (17) as

$$\begin{aligned} D_{n,n} &\approx ||\tilde{\mathbf{h}}_{\mathrm{b}}(0)||^2 \int_{-W/2}^{W/2} |\tilde{\psi}_n(W, f)|^2 \mathrm{d}f \\ &\approx M \sum_{s=1}^{N_{\mathrm{RF}}} \left| \alpha_{p(s)} \right|^2, \end{aligned} \tag{23}$$

$$\begin{aligned} D_{n,n'} &\approx ||\tilde{\mathbf{h}}_{\mathrm{b}}(0)||^2 \int_{-W/2}^{W/2} \tilde{\psi}_n^*(f) \tilde{\psi}_{n'}(f) \mathrm{d}f \\ &\approx 0, \end{aligned} \tag{24}$$

respectively, where (23) is based on the approximation $G(\check{\theta}_l(f) - \bar{\theta}_{g(s)})/M \approx 1$ for $l = p(s)$, $\int_{-W/2}^{W/2} |\tilde{\psi}_n(W, f)|^2 \mathrm{d}f \approx 1$, and (22); (24) is based on the fact that the OFDM subcarriers are almost orthogonal in the frequency domain $f \in [-W/2, W/2]$. Substituting (23) and (24) into (20) yields

$$\gamma_n \approx \frac{2\mathrm{E_x}}{N_0} M \sum_{s=1}^{N_{\mathrm{RF}}} \left| \alpha_{p(s)} \right|^2.$$

Then, we have

$$\mathbb{E}\{\gamma_n\} \approx \frac{2\mathrm{E_x}}{N_0} M N_{\mathrm{RF}} \sigma_\alpha^2. \tag{25}$$

By taking the expectation of (21) and substituting (25), we have

$$R \approx \log_2(1 + \frac{2\mathrm{E_x}}{N_0} M N_{\mathrm{RF}} \sigma_\alpha^2). \tag{26}$$

When the bandwidth W is wide enough such that $\check{\theta}_{p(s)}(f)$ is varies with the change of f in the domain $[-W/2, W/2]$, $||\tilde{\mathbf{h}}_{\mathrm{b}}(f)||^2$ in (22) also varies with f. By taking the expectation of $||\tilde{\mathbf{h}}_{\mathrm{b}}(f)||^2$, we have

$$\mathbb{E}\{||\tilde{\mathbf{h}}_{\mathrm{b}}(f)||^2\} \approx \frac{\sigma_\alpha^2}{M} \sum_{s=1}^{N_{\mathrm{RF}}} \left| G(\check{\theta}_{p(s)}(f) - \bar{\theta}_{g(s)}) \right|^2. \tag{27}$$

By taking the expectation of $D_{n,n}$ in (17) and substituting (27), we have

$$\begin{aligned} \mathbb{E}\{D_{n,n}\} \approx & \frac{\sigma_\alpha^2}{M} \sum_{s=1}^{N_{\mathrm{RF}}} \int_{-W/2}^{W/2} |\tilde{\psi}_n(W,f)|^2 \\ & \times \left| G(\check{\theta}_{p(s)}(f) - \bar{\theta}_{g(s)}) \right|^2 \mathrm{d}f. \end{aligned} \tag{28}$$

In the low signal-to-noise ratio (SNR) regime, i.e., when $\mathrm{E_x}/N_0$ is low, we can approximate (20) as

$$\gamma_n \approx \frac{2\mathrm{E_x} D_{n,n}}{N_0}. \tag{29}$$

By taking the expectation of (29) and substituting (28), we have

$$\begin{aligned} \mathbb{E}\{\gamma_n\} \approx & \frac{2\mathrm{E_x}\sigma_\alpha^2}{N_0 M} \sum_{s=1}^{N_{\mathrm{RF}}} \int_{-W/2}^{W/2} |\tilde{\psi}_n(W,f)|^2 \\ & \times \left| G(\check{\theta}_{p(s)}(f) - \bar{\theta}_{g(s)}) \right|^2 \mathrm{d}f \\ \approx & \frac{2\mathrm{E_x}\sigma_\alpha^2}{N_0 M} \sum_{s=1}^{N_{\mathrm{RF}}} \sum_{q=1}^{Q} \left| G(\check{\theta}_{p(s)}(f_q(W)) - \bar{\theta}_{g(s)}) \right|^2 \\ & \times \int_{f_{q-1}(W)}^{f_q(W)} |\tilde{\psi}_n(W,f)|^2 \mathrm{d}f, \end{aligned} \tag{30}$$

where $f_q(W) = -W/2 + qW/Q$, and the approximation is based on the fact that Q is large enough such that $G(\check{\theta}_{p(s)}(f) - \bar{\theta}_{g(s)}) \approx G(\check{\theta}_{p(s)}(f_q(W)) - \bar{\theta}_{g(s)})$, $\forall f_{q-1}(W) \leq f \leq f_q(W)$. According to (14), it is known that

$$\int_{f_{q-1}(W)}^{f_q(W)} |\tilde{\psi}_n(W,f)|^2 \mathrm{d}f = \int_{f_{q-1}(kW)}^{f_q(kW)} |\tilde{\psi}_n(kW,f)|^2 \mathrm{d}f, \tag{31}$$

where $k > 0$. In addition, according to (12), it is known that $|G(\check{\theta}_{p(s)}(f_q(W)) - \bar{\theta}_{g(s)})|$ generally decreases with the increase of $|\check{\theta}_{p(s)}(f_q(W)) - \bar{\theta}_{g(s)}|$. As $|\check{\theta}_{p(s)}(0) - \bar{\theta}_{g(s)}| \approx 0$, we have

$$|\check{\theta}_{p(s)}(f_q(W)) - \bar{\theta}_{g(s)}| < |\check{\theta}_{p(s)}(f_q(kW)) - \bar{\theta}_{g(s)}|, \forall k > 1.$$

Thus, $|G(\check{\theta}_{p(s)}(f_q(W)) - \bar{\theta}_{g(s)})|$ is usually larger than $|G(\check{\theta}_{p(s)}(f_q(kW)) - \bar{\theta}_{g(s)})|$ for $k > 1$. Based on this fact and (30), (31), we know that $\mathbb{E}\{\gamma_n\}$ generally decreases with the increase of W. By taking the expectation of (21), we have $R \approx \frac{1}{N} \sum_{n=1}^{N} \log_2(1 + \mathbb{E}\{\gamma_n\})$. Thus, the spectral efficiency generally decreases with the increase of the bandwidth W.

This effect is known as the beam squint effect in wideband mm-wave systems with a large antenna array. As the bandwidth W and the number of antennas M are large, we have $f_q(W) \gg 0$. Then, $|\check{\theta}_{p(s)}(f_q(W)) - \bar{\theta}_{g(s)}| \gg 0$, which means the beam direction goes away from the path direction. Thus, the array gain $G(\check{\theta}_{p(s)}(f) - \bar{\theta}_{g(s)})$ for frequency away from the carrier frequency is not high enough.

When the number of subcarriers N is large enough such that $\check{\theta}_{p(s)}(f)$ is almost invariant with the change of f in the domain $[f_n - 5B, f_n + 5B]$, where $\tilde{\psi}_n(W,f) \approx 0$ for $f \notin [f_n - 5B, f_n + 5B]$, we can approximate (17) as

$$\begin{aligned} D_{n,n} &\approx ||\tilde{\mathbf{h}}_{\mathrm{b}}(f_n)||^2 \int_{-W/2}^{W/2} |\tilde{\psi}_n(W,f)|^2 \mathrm{d}f \\ &\approx ||\tilde{\mathbf{h}}_{\mathrm{b}}(f_n)||^2, \\ D_{n,n'} &\approx ||\tilde{\mathbf{h}}_{\mathrm{b}}(f_n)||^2 \int_{-W/2}^{W/2} \tilde{\psi}_n^*(f) \tilde{\psi}_{n'}(f) \mathrm{d}f \\ &\approx 0. \end{aligned}$$

respectively, where the second approximation is based on the approximation $\int_{-W/2}^{W/2} |\tilde{\psi}_n(W,f)|^2 \mathrm{d}f \approx 1$, the forth approximation is based on the fact that the OFDM subcarriers are almost orthogonal in the frequency domain $f \in [-W/2, W/2]$. Substituting these approximations into (20) yields

$$\gamma_n \approx \frac{2\mathrm{E_x}}{N_0} ||\tilde{\mathbf{h}}_{\mathrm{b}}(f_n)||^2.$$

As can be seen, the interference decreases with the increase of the number of subcarriers.

IV. Simulation Results

In this section, we compare the spectral efficiency in (21) and the approximate spectral efficiency in (26). In addition, we also compare an upper bound of the spectral efficiency, which is calculated without the interference as

$$R_{\mathrm{Up}} = \frac{1}{N} \sum_{n=1}^{N} \mathbb{E}\{\log_2(1 + \tilde{\gamma}_n)\}, \tag{32}$$

where $\tilde{\gamma}_n = 2\mathrm{E_x} D_{n,n}/N_0$. In the simulations, the SNR of the system is defined as $\mathrm{E_x}/N_0$ and is -10 dB. The number of subcarriers is $N = 256$. The system bandwidth is $W = 0.02 f_{\mathrm{c}}$. The carrier frequency is $f_{\mathrm{c}} = 60$ GHz. The DOAs $\phi_l, l = 1, 2, \cdots, L$ are uniformly distributed in the range $[0, 2\pi]$. The time delays $\tau_l, l = 1, 2, \cdots, L$ are uniformly distributed in the range $[0, 256/W]$. The variance of the path gain is $\sigma_\alpha^2 = 1$. The number of BS antennas is $M = 61$. The number of paths is $L = 8$. The number of RF chains is $N_{\mathrm{RF}} = 4$. The distance between adjacent BS antennas is $d = 0.5\lambda$.

Fig. 2 describes the changes in spectral efficiency under different SNRs. It can be seen that when the SNR is lower than -10 dB, the spectral efficiency is very close to the upper bound. This is because the interference has limited effects on the spectral efficiency when the SNR is low. It can also be seen that the spectral efficiency is close to the approximation

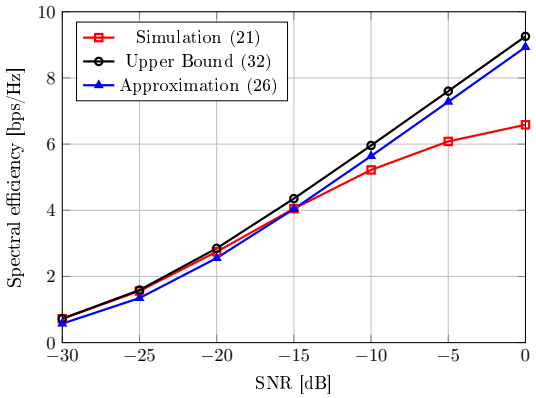

Fig. 2. The spectral efficiency versus the SNR.

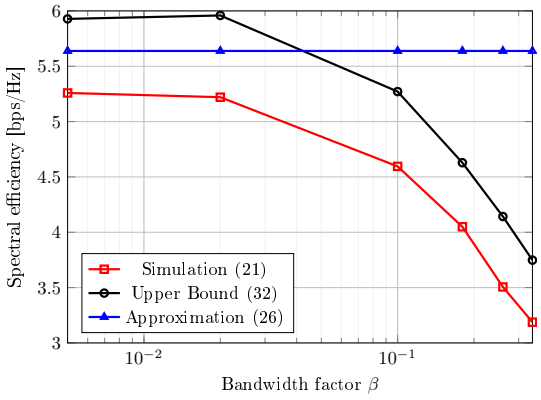

Fig. 3. The spectral efficiency versus the bandwidth.

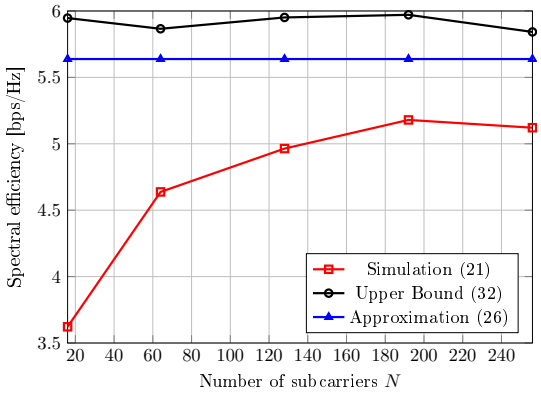

Fig. 4. The spectral efficiency versus the number of subcarriers.

when the SNR is lower than -10 dB. This is verifies that the approximation for the narrow bandwidth case is of little error for the low SNR case. When the SNR is higher than -10 dB, the spectral efficiency begins to saturate, while the approximation still increases. This is because the interference term in (24) is amplified by the high SNR and is not negligible in comparison to the noise power in (20).

Fig. 3 shows the spectral efficiency changes with bandwidth factor β, in which the bandwidth is $W = \beta f_c$. It can be seen that when the bandwidth increases, the spectral efficiency and the upper bound decreases. This is because the beam squint effect becomes serious. Moreover, the spectral efficiency is close to the approximation when the bandwidth is narrow and is away from the approximation when the bandwidth is wide. This is because the approximation is based on the assumption that the bandwidth is narrow. These results verifies the analysis about the effect of the bandwidth in Sec. III.

Fig. 4 shows the spectral changes with the number of subcarriers. When the number of subcarriers increases, it can be seen that the spectral efficiency increases and gets close to the approximation and the upper bound. This result verifies the analysis about the effect of the number of subcarriers in Sec. III, which shows the interference decreases with the increase of the number of subcarriers. It can also be observed in Fig. 3 and Fig. 4 that there is difference between the spectral efficiency and the approximation when $\beta = 0.005$ or $N = 256$. This is because the OFDM subcarriers are not exactly orthogonal, especially for subcarriers that are close in frequency, which means $D_{n,n'} \neq 0, \forall n \neq n'$.

V. Conclusion

In this paper, we analyzed the spectral efficiency of wideband mm-wave OFDM systems with a large antenna array at the BS. The analysis and the simulation show that the wide bandwidth makes the beam points to a direction away from the path, i.e., causes the beam squint effect. We show that by increasing the number of subcarriers the beam squint effect can be alleviated.

References

[1] J. Rodríguez-Fernández and N. González-Prelcic, "Channel estimation for frequency-selective mmWave MIMO systems with beam-squint," in *Proc.2018 IEEE Global Commun. Conf. (GLOBECOM)*, Abu Dhabi, United Arab Emirates, Dec. 2018, pp. 1–6,

[2] X. Gao, L. Dai, S. Zhou, A. M. Sayeed, and L. Hanzo, "Wideband beamspace channel estimation for millimeter-wave MIMO systems relying on lens antenna arrays," *IEEE Trans. Signal Process.*, vol. 67, no. 18, pp. 4809–4824, Sep. 2019.

[3] B. Wang, F. Gao, S. Jin, H. Lin, and G. Y. Li, "Spatial- and frequency-wideband effects in millimeter-wave massive MIMO systems", *IEEE Trans. Signal Process.*, vol. 66, no. 13, pp. 3393–3406, Jul. 2018.

[4] B. Wang, F. Gao, S. Jin, H. Lin, G. Y. Li, S. Sun, and T. S. Rappaport, "Spatial-wideband effect in massive MIMO with application in mmWave systems", *IEEE Commun. Mag.*, vol. 56, no. 12, pp. 134–141, Dec. 2018.

[5] J. H. Brady and A. M. Sayeed, "Wideband communication with high-dimensional arrays: New results and transceiver architectures," in *Proc. 2015 IEEE Int. Conf. Commun. Workshop (ICCW)*, London, UK, Jun. 2015, pp. 1042–1047.

[6] A. Alkhateeb, G. Leus, and R. W. Heath, Jr., "Limited feedback hybrid precoding for multi-user millimeter wave systems," *IEEE Trans. Commun.*, vol. 14, no. 11, pp. 6481–6494, Nov. 2015.

[7] K. Venugopal, N. González-Prelcic, and R. W. Heath, Jr., "Optimality of frequency flat precoding in frequency selective millimeter wave channels," *IEEE Wireless Commun. Lett.*, vol. 6, no. 3, pp. 330–333, Jun. 2017.

[8] G. C. Ferrante, T. Q. S. Quek, and M. Z. Win, "Revisiting the capacity of noncoherent fading channels in mmWave system," *IEEE Trans. Commun.*, vol. 65, no. 8, pp. 3259–3275, Aug. 2017.

[9] D. Zhang, Z. Zhou, C. Xu, Y. Zhang, J. Rodriguez, and T. Sato, "Capacity analysis of NOMA with mmWave massive MIMO systems," *IEEE J. Sel. Areas Commun.*, vol. 35, no. 7, pp. 1606–1618, Jul. 2017.